Remote Sensing of Environment 167 (2015) 78–87

Contents lists available at ScienceDirect

Remote Sensing of Environment

journal homepage: www.elsevier.com/locate/rse

Remotely estimating photosynthetic capacity, and its response to temperature, in vegetation canopies using imaging spectroscopy

Shawn P. Serbin [a,*], Aditya Singh [b], Ankur R. Desai [c], Sean G. Dubois [c], Andrew D. Jablonski [b], Clayton C. Kingdon [b], Eric L. Kruger [b], Philip A. Townsend [b]

[a] Biological, Environmental, and Climate Sciences Department, Brookhaven National Laboratory, Upton, NY11973-5000, USA
[b] Department of Forest & Wildlife Ecology, University of Wisconsin-Madison, Madison, WI53706, USA
[c] Department of Atmospheric and Oceanic Sciences, University of Wisconsin-Madison, Madison, WI53706, USA

ARTICLE INFO

Article history:
Received 6 April 2015
Received in revised form 24 May 2015
Accepted 27 May 2015
Available online 11 June 2015

Keywords:
Activation energy
AVIRIS
Imaging spectroscopy
Canopy optical reflectance
Photosynthesis
Temperature
V_{cmax}
Photosynthetic metabolism

ABSTRACT

To date, the utility of ecosystem and Earth system models (EESMs) has been limited by poor spatial and temporal representation of critical input parameters. For example, EESMs often rely on leaf-scale or literature-derived estimates for a key determinant of canopy photosynthesis, the maximum velocity of RuBP carboxylation (V_{cmax}, μmol m^{-2} s^{-1}). Our recent work (Ainsworth et al., 2014; Serbin et al., 2012) showed that reflectance spectroscopy could be used to estimate V_{cmax} at the leaf level. Here, we present evidence that imaging spectroscopy data can be used to simultaneously predict V_{cmax} and its sensitivity to temperature (E_V) at the canopy scale. In 2013 and 2014, high-altitude Airborne Visible/Infrared Imaging Spectroscopy (AVIRIS) imagery and contemporaneous ground-based assessments of canopy structure and leaf photosynthesis were acquired across an array of monospecific agroecosystems in central and southern California, USA. A partial least-squares regression (PLSR) modeling approach was employed to characterize the pixel-level variation in canopy V_{cmax} (at a standardized canopy temperature of 30 °C) and E_V, based on visible and shortwave infrared AVIRIS spectra (414–2447 nm). Our approach yielded parsimonious models with strong predictive capability for V_{cmax} (at 30 °C) and E_V (R^2 of withheld data = 0.94 and 0.92, respectively), both of which varied substantially in the field (≥1.7 fold) across the sampled crop types. The models were applied to additional AVIRIS imagery to generate maps of V_{cmax} and E_V, as well as their uncertainties, for agricultural landscapes in California. The spatial patterns exhibited in the maps were consistent with our in-situ observations. These findings highlight the considerable promise of airborne and, by implication, space-borne imaging spectroscopy, such as the proposed HyspIRI mission, to map spatial and temporal variation in key drivers of photosynthetic metabolism in terrestrial vegetation.

1. Introduction

Modeling global change requires accurate representation of terrestrial carbon, energy and water fluxes. The current generation of Ecosystem and Earth System Models (EESMs) fail to adequately capture the magnitude, spatial variation, and seasonality of gross primary productivity (GPP), resulting in a critical uncertainty in the size and fate of the terrestrial carbon sink (Friedlingstein et al., 2014). At a fundamental level, EESMs rely on detailed parameterization of vegetation functional traits (e.g., those describing photosynthesis, Bernacchi et al., 2013) to represent ecosystem processes of a given biome. These trait data are typically sourced from the literature or field campaigns (e.g. Dietze et al., 2014), often from a single site or study, and provide an incomplete spatial and temporal characterization of key vegetation properties. In application, literature- or field-derived estimates are partitioned into between five and sixteen discrete plant functional types (PFTs) that describe variation of these traits across the entire planet (Rogers, 2014; Wullschleger et al., 2014).

In response to the compromises that generalization by PFTs incurs, there is increasing interest in the development of novel approaches to use optical remote sensing to map variability in physiological function and biochemistry of terrestrial vegetation at broad spatial and temporal scales (e.g., Frankenberg et al., 2014; Guanter et al., 2014; Singh, Serbin, McNeil, Kingdon, & Townsend, in press; Zhang et al., 2014; Zhou et al., 2014). Of critical importance is the ability to accurately estimate the spatial and temporal variability in the photosynthetic capacity of vegetation canopies, which is governed in large part by V_{cmax}, the maximum rate at which the enzyme rubisco catalyzes the carboxylation of RuBP in leaf chloroplasts (Bernacchi et al., 2013; Farquhar, von Caemmerer, & Berry, 1980). V_{cmax} is a key parameter in most models of land–atmosphere carbon, energy and water exchange (e.g., Kucharik et al., 2000; Medvigy, Wofsy, Munger, Hollinger, & Moorcroft, 2009;

* Corresponding author.
E-mail address: sserbin@bnl.gov (S.P. Serbin).

http://dx.doi.org/10.1016/j.rse.2015.05.024
0034-4257/

Rogers, 2014; Schaefer et al., 2012). Moreover, on its own, V_{cmax} can serve as a useful bioindicator, given its pronounced responsiveness to a number of common biotic and abiotic stressors, such as insect or pathogen damage (Dungan, Turnbull, & Kelly, 2007), air pollution (e.g., Ainsworth et al., 2014), drought (e.g., Xu & Baldocchi, 2003) and climatic extremes (Weston & Bauerle, 2007).

Even in the absence of stress, V_{cmax} is known to display significant variation across species, seasons, functional groups and climates (Dillaway & Kruger, 2010; Kattge & Knorr, 2007; Sage, Way, & Kubien, 2008; Wullschleger, 1993; Wilson, Baldocchi, & Hanson, 2000). Inaccurate characterization of this variation limits the direct use of leaf-level V_{cmax} in modeling and other applications. One important source of V_{cmax} variation is leaf temperature (Leuning, 2002; Kattge & Knorr, 2007; Medlyn, Dreyer, Ellsworth, et al., 2002a). Specifically, V_{cmax} exhibits an exponential sensitivity to temperature that is typically quantified in terms of activation energy (E_V), derived from the Arrhenius equation (e.g., Hikosaka, Ishikawa, Borjigidai, Muller, & Onoda, 2006; Leuning, 2002). As with V_{cmax}, E_V has been shown to vary substantially across plant functional types (Dillaway & Kruger, 2010; Kattge & Knorr, 2007; Sage et al., 2008). Presently, however, there is no compelling empirical or theoretical model to account for this observed variation (Hikosaka et al., 2006; Sage et al., 2008), and E_V therefore requires explicit parameterization within models for each PFT from the limited observations available.

Recent work (Ainsworth et al., 2014; Dillen, Op de Beeck, Hufkens, Buonanduci, & Phillips, 2012; Doughty et al., 2011; Serbin et al., 2012) highlighted that reflectance spectroscopy can be used to estimate leaf-level V_{cmax}. Importantly, Serbin et al. (2012) also showed that the spectroscopic approach could characterize variation in V_{cmax} related to growth environment (e.g., temperature) more effectively than the simple physiological scaling with leaf nitrogen concentration (%N), leaf mass per area (LMA), or the combination of the two (N_{area}, g m^{-2}; Domingues et al., 2010; Kattge, Knorr, Raddatz, & Wirth, 2009; Niinemets, Cescatti, Rodeghiero, & Tosens, 2006). The findings by Serbin et al. (2012) provide the potential for real-time regional monitoring of photosynthetic metabolism through the use of portable spectrometers as well as imaging spectrometers like the Airborne Visible/Infrared Imaging Spectrometer (AVIRIS; Green, Eastwood, Sarture, et al., 1998). NASA's proposed satellite-borne Hyperspectral Infrared Imager (HyspIRI, Roberts, Quattrochi, Hulley, Hook, & Green, 2012) — a two-sensor system with a 400–2500 nm imaging spectrometer plus a multi-spectral thermal instrument — would provide regular (19 day return interval) and global scale monitoring of these important time- and space-varying traits. Incorporation of such spatially and temporally rich datasets, in model initialization, parameterization, and evaluation of prognostic model outputs, could significantly improve the ability of EESMs to project vegetation carbon uptake and storage.

In this study, we evaluated the ability of imaging spectroscopy data from AVIRIS-Classic (Green et al., 1998; referred to as AVIRIS from this point forward) to estimate V_{cmax}, as well as its temperature sensitivity, E_V, in managed crop canopies. In 2013 and 2014, high-altitude AVIRIS imagery and contemporaneous ground-based assessments of leaf photosynthesis were acquired on multiple dates across a diverse set of monospecific agroecosystems in central and southern California, USA. Partial least-squares regression (PLSR) modeling was employed to predict V_{cmax} (at a standardized canopy temperature of 30 °C) and E_V from field measurements, estimates of canopy cover and 414–2447 nm AVIRIS spectra. We estimated error and uncertainty through split-sample cross-validation of 500 permutations of the data (Singh et al., in press). To further assess the credibility and applicability of the resulting algorithms, we applied the models to additional AVIRIS images in agricultural areas of California to map V_{cmax} and E_V, as well as their uncertainties, to examine whether the predictions fell within the range of expectations and produced coherent maps.

2. Methods

2.1. Description of vegetation sampling sites

This research was conducted during spring (March–April) and early summer (June) in 2013 and 2014. Our study region consisted of the complex agricultural matrix of the Imperial and San Joaquin Valleys of California (Fig. 1). Within this area, a number of economically important food crops are grown for domestic consumption and export. Given the global importance of this food-producing region, better approaches for monitoring crop health and status are critical in the face of continued global climate change and population growth (Ainsworth, Rogers, & Leakey, 2008).

Our sampling sites (Fig. 1) were located at three University of California agricultural research stations (Table 1). These stations fell within the footprint of NASA's HyspIRI prototyping airborne campaign in which more than 25% of California was imaged at three time points in each year of the study. At each site, we selected irrigated, monospecific C_3 agroecosystems that were large enough to contain multiple 18 m AVIRIS pixels. Over two years, we sampled a total of 9 different crop species in 13 different agroecosystems, across four measurement campaigns. As a result, we obtained field data aligned with six AVIRIS images throughout our study period (Table 1).

2.2. Field data

Vegetation cover and physiological traits were generally collected within one week of AVIRIS overflights in the spring and early summer of 2013 and 2014. In cases with longer intervals between ground-based campaigns and overflights, we ensured that the following conditions were met: 1) the vegetation was mature (i.e. at peak biomass) at both the time of sampling and overflight, and 2) there was no obvious trend in either temperature or precipitation over the period between sampling and overflights that might have significantly altered vegetation structure or physiology. Moreover, this timeframe did not span any seasonal transitions. Because these agroecosystems were irrigated, delays between measurements and overflights likely had less of an impact on the ability to accurately characterize physiological functioning (i.e. compared to natural vegetation in water-limited environments).

2.2.1. Ground-based measures of vegetation cover

At different sampling locations within each agroecosystem, we measured percent canopy cover and leaf area index (LAI) using a point-intercept method (Wilson, 2011). For taller canopies, we used the "rods as points" method, moving a fine diameter pole through the canopy. For shorter-stature vegetation, we utilized a traditional approach of dropping the rod into the canopy from above (Wilson, 2011). For taller orchard sites, we also used a densitometer to provide an additional estimate of canopy cover. Point intercept measurements were made at 1 m increments on two crossing, 30 m transects stretched at a random angle across the ecosystem. All sample locations were recorded using GPS.

2.2.2. Measurement of V_{cmax} and E_V at the leaf level

We measured leaf gas exchange on the target species in each of the 13 agroecosystems (Table 1) using a LI-6400 portable photosynthesis system combined with the 6400–40 leaf chamber fluorometer (Li-Cor Biosciences, Lincoln, NE, USA). At representative plots distributed within each site, we measured gas exchange on attached, mature, sunlit foliage located in the upper third of the vegetation canopy. For taller orchard trees, we utilized tall tripods or platforms to reach the upper third of the canopies. Leaves were measured under high light intensities (photosynthetic photon flux = 2000 μmol m^{-2} s^{-1}, provided by a red-blue LED array) at a cuvette CO_2 partial pressure (pCO_2) ranging from 7.5 to 25 Pa. At a particular cuvette reference pCO_2, which was controlled using the LI-6400 CO_2 injector system, leaves were allowed

Fig. 1. Study area map. Location of agricultural sampling locations in California indicated by triangle symbols. KARE = Kearney Agricultural Extension and Research Center, Parlier, CA; SCREC = South Coast Research and Extension Center, Irvine, CA; CVARS = Coachella Valley Agricultural Research Station, Thermal, CA.

to acclimate for 2–10 min prior to measurement. We monitored, but did not control, vapor pressure deficit (VPD) between leaf and air in the cuvette, which ranged from 1.4 to 2.1 kPa.

Characterization of E_V, the temperature response of V_{cmax}, requires data to model leaf photosynthetic pCO_2 responses across the range of temperatures experienced by a plant at a location. We thus made measurements to calculate V_{cmax} at three reference cuvette temperatures (e.g., 20, 28 and 35 °C). The intent of this protocol was to generate photosynthetic pCO_2 responses across a leaf temperature range of at least 10 °C, which facilitated an accurate estimate of E_V (e.g. Medlyn, Loustau, & Delzon, 2002b). This approach allowed us to estimate V_{cmax} at a range of canopy temperatures that encompassed those observed during the time of AVIRIS overflights. At a given leaf temperature, the observed relationship between photosynthesis (A) and intercellular pCO_2 (C_i) was used to estimate V_{cmax}, employing a trend-fitting method that minimized the total sums of squares for differences between observed versus predicted A (Long & Bernacchi, 2003). Estimates incorporated Michaelis–Menten constants for CO_2 (K_c) and oxygen (K_o), as well as photosynthetic compensation pCO_2 (Γ^*), derived using formulae from Long and Bernacchi (2003). Finally, our approach did not account for the influence of mesophyll conductance on CO_2 diffusion into the chloroplast (Dillaway & Kruger, 2010), thus our reported V_{cmax} values are "apparent" (Bernacchi et al., 2013) and based on C_i as opposed to chloroplastic pCO_2 (C_c).

For each monospecific agroecosystem, E_V was modeled based on data pooled across all sampled leaves and cuvette temperatures. Since the observed temperature response of V_{cmax} was exponential in all cases, E_V was modeled using an Arrhenius equation (Dillaway & Kruger, 2010; Hikosaka et al., 2006; Medlyn, Dreyer, et al., 2002a; Serbin et al., 2012). The resulting models produced unbiased estimates of V_{cmax} for all target species and measurement dates. Namely, the slopes and intercepts of relationships between observed and predicted V_{cmax} did not differ significantly from 1 and 0, respectively (data not shown).

2.3. Image data and processing

AVIRIS images covering sites of our ground-based measures of canopy structure and leaf gas exchange were acquired from NASA's ER-2 aircraft flown at approximately 20 km altitude. The 18 m-pixel images were radiometrically calibrated to surface reflectance by NASA Jet Propulsion Laboratory using the modified ATREM atmospheric correction described by Thompson et al. (2015). For all ensuing analyses, we omitted the atmospheric water absorption bands (1313–1453 nm and 1782–2018 nm), as well as the five shortest and longest wavebands, which exhibited unacceptable levels of noise. Our analyses used 172 of the 224 channels of AVIRIS data over the 414–2447 nm range. Locations of ground measurements were identified within AVIRIS images using GPS data, and spectra were extracted only from pixels that fell entirely within the target agroecosystems. The total sample size for our analysis was 72.

AVIRIS imagery can exhibit between- and within-scene variations in brightness due to topography and bidirectional reflectance effects resulting from varying earth–sun-sensor geometry. We performed a brightness correction across all pixels on all images, following Feilhauer, Asner, Martin, and Schmidtlein (2010), to normalize between- and within-scene brightness offsets. This method preserves the overall shape of spectral vectors for individual pixels while removing whole-scene systematic brightness offsets.

We extracted brightness-normalized reflectance spectra for ground locations in which V_{c30}, E_V and vegetation cover measurements

Table 1
All agroecosystems sampled in 2013 and 2014 were located on University of California research stations: Coachella Valley Agricultural Research Station (CVARS), Kearney Agricultural Research & Extension Center (KARE), South Coast Research & Extension Center (SCREC). Here we provide means (± standard deviation) for V_{cmax} at 30 °C (V_{c30}) and E_v based on leaf gas exchange measurements. We also provide the number of pixels extracted from a particular agroecosystem for AVIRIS image analysis.

Species	Location	Measurement date	Image date	V_{c30} ± Std Dev	E_v ± Std Dev	Number of pixels
Avocado	SCREC	3/22/13	4/19/13	124.4 ± 5.4	67.4 ± 8.5	2
Grape	CVARS	6/7/13	5/22/13	111.5 ± 11.7	62.7 ± 11.8	5
Lemon	CVARS	4/17/14	4/14/14	83.1 ± 5.2	103.7 ± 14.2	2
Oat (mature)	KARE	4/10/14	4/7/14	219.7 ± 10.1	86.0 ± 9.0	5
Oat (young)	KARE	4/11/14	4/7/14	190.9 ± 9.4	75.9 ± 9.2	4
Palm	CVARS	4/16/14	4/14/14	83.1 ± 5.2	103.7 ± 14.2	4
Palm	CVARS	6/5/14	6/13/14	93.1 ± 17.9	88.2 ± 17.9	5
Peach	KARE	4/9/14	4/7/14	176.2 ± 12.8	67.2 ± 12.1	5
Pistachio	KARE	6/26/13	5/03/13	234.9 ± 15.3	79.2 ± 6.3	5
Pomegranate	KARE	4/12/14	4/7/14	112.4 ± 5.5	105.1 ± 14.4	4
Red pepper	CVARS	6/5/13	5/22/13	216.3 ± 7.5	71.9 ± 7.1	10
Red pepper	CVARS	4/15/14	4/14/14	174.1 ± 5.9	78.0 ± 4.1	10
Red pepper	CVARS	6/6/14	6/13/14	123.8 ± 5.9	78.0 ± 4.1	9

had been acquired. The parameters V_{c30} and E_V refer to the metabolic capacity of vegetation within these pixels, but the pixels themselves include both vegetation and soil. From a pixel-based perspective, the V_{c30} (or E_V) that is "seen" in a pixel is for the top layer of leaves within that pixel, namely the foliage that is exposed to the sensor. Areas with no vegetation cover (i.e. exposed bare soil) have no V_{c30} or E_V. Since every pixel is mixed, we consequently must distinguish the V_{c30} and E_V of the vegetation canopy surface within a given pixel from the V_{c30} and E_V of the pixel itself, referring to the latter as $V_{c30,pixel}$ and $E_{v,pixel}$. For analysis, we modified ground-based measurements of V_{c30} and E_v by fractional vegetation cover as:

1) $V_{c30,pixel} = V_{c30} *$ fractional cover;
2) $E_{V,pixel} = E_V *$ fractional cover.

To map $V_{c30,pixel}$ and $E_{V,pixel}$, we needed accurate pixel-level estimates of fractional vegetation cover across several scenes. We used our vegetation sampling data as well as cover estimates derived from high-resolution Google Earth images (sourced variously January–May, 2015; original image source: Digital Globe) to estimate cover as a function of the AVIRIS imagery. We randomly selected ~300 locations in each of the six AVIRIS images and overlaid a 7 × 7 sampling grid (3 m spacing) on high-resolution Google Earth imagery (dated within 5 days of AVIRIS overflights). We visually interpreted each of the 49 grid intersections as green vegetation, shadow, non-photosynthetic vegetation, bare soil/rock or other. We extracted the 49 spectra each from these 300 sampling locations, averaged ones that were maximally represented in each class at each sampling grid (>95% grid intersections of the class), and used them as 'pure' endmembers to generate maps of spectral angles (Kruse et al., 1993) using the spectral angle mapper utility in ENVI (v. 4.8, Exelis, McLean, VA).

To estimate fractional vegetation cover, we tested various combinations of inputs (i.e. soil, green vegetation, shadow spectral angles) in a logistic regression framework. The most parsimonious model utilized only soil spectral angles and was able to explain over 90% of the variation in measured canopy cover (Fig. S1). The models involved 500 permutations of the data with a 75%/25% split for calibration and validation. We mapped fractional cover as the median response of the 500 permutations, and mapped the uncertainty in those estimates as the standard deviation of all permutations. This method for mapping a trait and its uncertainty, which is outlined in Singh et al. (in press), allowed us to account for error in our mapping and modeling, spatially, while performing error propagation as we integrated data for mapping our ultimate response variables, $V_{c30,pixel}$ and $E_{V,pixel}$.

2.4. Estimation of $V_{c30,pixel}$ and $E_{V,pixel}$ with their uncertainties

We used the empirical partial least square regression (PLSR, see Geladi & Kowalski, 1986; Wold, Ruhe, Wold, & Dunn, 1984; Wold, Sjostrom, & Eriksson, 2001) modeling approach to build the relationships between $V_{c30,pixel}$ and $E_{V,pixel}$ and AVIRIS reflectance spectra. Our application of PLSR is described in detail by Singh et al. (in press), with other uses in imaging spectroscopy covered by a range of authors (e.g., Asner, Martin, Anderson, & Knapp, 2015; Dahlin, Asner, & Field, 2013; Martin, Plourde, Ollinger, Smith, & McNeil, 2008). Briefly, PLSR iteratively transforms predictor (here: brightness-normalized spectra) and response variables (either $V_{c30,pixel}$ or $E_{V,pixel}$) to identify latent vectors and generate bandwise calibration factors used to create a predictive linear model. PLSR works to maximize covariance between independent and dependent variables, while maintaining orthogonality in the factors derived from spectra. PLSR is preferable to methods such as stepwise regression that yield spurious relationships or poor validation due to overfitting (Grossman et al., 1996). We implemented 500 permutations of the PLSR analysis, with 25% of the data in each permutation randomly assigned to validation and the remaining 75% to calibration. For each permutation of the model, we perturbed the response variable ($V_{c30,pixel}$, $E_{V,pixel}$), within 95% of its respective error estimate, weighted this new estimate with a perturbed estimate of the vegetation fraction (obtained by a similarly randomized cover fraction model), and refit the PLSR model. This approach enabled us to propagate errors from every preceding step of our analyses. Thus, we report the model coefficients of the 500 randomized (and perturbed) models as jackknifed 95% confidence intervals. From this analysis, we also report the median R^2 obtained by applying coefficients from the 500 models to image spectra, as well as the validation R^2 of the 500 sets of withheld data. Additionally, we report the root mean square errors (RMSE) of each model fit statistic, as well as the RMSE as a proportion of the range of data.

We plot standardized PLSR coefficients and the Variable Importance of Projection statistic (VIP, Wold, 1994) to identify the direction of effect by wavelength (standardized coefficients) and relative importance (VIP) of different wavelengths to the PLSR predictions (e.g. Serbin, Singh, McNeil, Kingdon, & Townsend, 2014). The mean coefficients and variability in those coefficients across the 500 permutations facilitate interpretation of the PLSR results with respect to known spectral associations at different wavelengths. We report the standardized coefficients (Fig. 3), as opposed to raw coefficients, to facilitate the comparison of the relative contribution to the PLSR across wavelengths; this was necessitated by the variability in average vegetation reflectance in different spectral ranges, e.g., with the visible being dark and having low average reflectance and the NIR comparatively bright. However, we utilized the raw coefficients with the brightness-normalized imagery for generating the maps of $V_{c30,pixel}$ and $E_{V,pixel}$.

2.5. Mapping $V_{c30,pixel}$ and $E_{v,pixel}$

We mapped $V_{c30,pixel}$ and $E_{V,pixel}$ as the mean of predictions obtained by applying the full set of 500 randomly permuted PLSR coefficients on each AVIRIS image on a pixel-wise basis. Uncertainties are presented here as the standard deviations of the 500 predictions. Higher uncertainties indicate conditions that fall increasingly outside the realm of our measurements.

3. Results

Across agroecosystems in this study, the ground-based, leaf-level estimates of V_{c30} and E_V displayed a variation of 2.8 fold (83–234 μmol m^{-2} s^{-1}) and 1.7 fold (62–105 kJ mol^{-1} K^{-1}), respectively (Table 1). Our observations of fractional vegetation cover ranged from 0.04 to 0.94, with the lowest in areas of exposed soil or sand and the highest corresponding to areas with the greatest cover of different crop types. To derive our $V_{c30,pixel}$ from the measured V_{c30}, a logistic model was used to estimate per-pixel vegetation cover. The resulting model displayed generally good results for unmixing, with a validation-$R^2 = 0.92$ and a RMSE = 10% (cross-validated on withheld data) of the range in fractional cover (results and model coefficients shown in Supplemental Fig. S1). The resulting V_{c30} adjusted by observed canopy cover ($V_{c30,pixel}$, downweighted to account for exposed soil fraction) ranged from 16 to 212 μmol m^{-2} (ground area) s^{-1}. We followed the same approach to derive $E_{V,pixel}$ from E_V, with a resulting $E_{V,pixel}$ range from 15 to 82 kJ mol^{-1} K^{-1}.

Cross-validation from the PLSR modeling indicated that 94% of the variation in $V_{c30,pixel}$ and 92% of the variation in $E_{V,pixel}$ were explained by algorithms derived from AVIRIS spectra (Table 2, Fig. 2). Moreover, AVIRIS-based PLSR models for $V_{c30,pixel}$ and $E_{V,pixel}$ were reasonably precise and parsimonious, as their root mean square errors were roughly 6% of the dependent variable data range (RMSE = 11.6 μmol m^{-2} s^{-1} for $V_{c30,pixel}$, and 4.4 kJ mol^{-1} K^{-1} for $E_{V,pixel}$, Fig. 2), and they required only three and seven latent components, respectively, to achieve this predictive capability.

We analyzed the standardized PLSR coefficients and VIP statistics to assess possible relationships between canopy spectra and our measures of leaf physiology (Fig. 3). The analyses revealed that the $V_{c30,pixel}$ and

$E_{V,pixel}$ models generally utilized all regions of the electromagnetic spectrum, but with key differences in important wavelengths as well as the direction (i.e. the sign) of the PLSR standardized coefficients. For example, shortwave infrared (SWIR, >1300 nm) reflectance was important to the estimation of both parameters, while visible (400–700 nm) and Near-infrared (NIR) wavelengths (1150–1300 nm) were especially influential in the $V_{c30,pixel}$ model. On the other hand the 1000–1150 nm and SWIR wavelengths around 1500–1700 nm appeared to be more important for the $E_{V,pixel}$ model. Notably, relationships with physiological parameters are suggested by the PLSR coefficients and VIPs in the far-red region for both models. In the $V_{c30,pixel}$ model, a strong local peak in standardized coefficient and VIP values occurred at 743 nm. In the $E_{V,pixel}$ model, a large negative coefficient coincided with a high VIP at a slightly shorter wavelength at the red-edge (~724 nm). The VIP statistics indicate that, for the most part, the entire spectral range (especially the SWIR) is important to the prediction of $V_{c30,pixel}$ and $E_{V,pixel}$.

To further evaluate the credibility and general applicability of our $V_{c30,pixel}$ and $E_{V,pixel}$ models, we made maps using the full suite of HyspIRI campaign AVIRIS images for our study region (Fig. 1), as illustrated for two 25-km^2 agricultural mosaics in central and southern California (Fig. 4). The resulting maps of $V_{c30,pixel}$ and $E_{V,pixel}$ estimates—when compared with AVIRIS false-color composites, our mapped fractional vegetation cover and NLCD land cover maps—show a broad range of spatiotemporal variation and are consistent with cover-weighted conversions of our canopy estimates. Of note, the resulting maps show marked variation in $V_{c30,pixel}$ and $E_{V,pixel}$ (and fractional cover), and the absence of any consistent relationship between canopy surface V_{c30} and E_V (Table 1). Uncertainty maps for $V_{c30,pixel}$ and $E_{V,pixel}$ and fractional cover illustrate locations where the predictive equations likely yield the greatest errors. Areas of high uncertainties occur largely near field edges and areas of vegetation cover <30%. Spatial variations in uncertainty rarely exceeded 10% of the range of the input data.

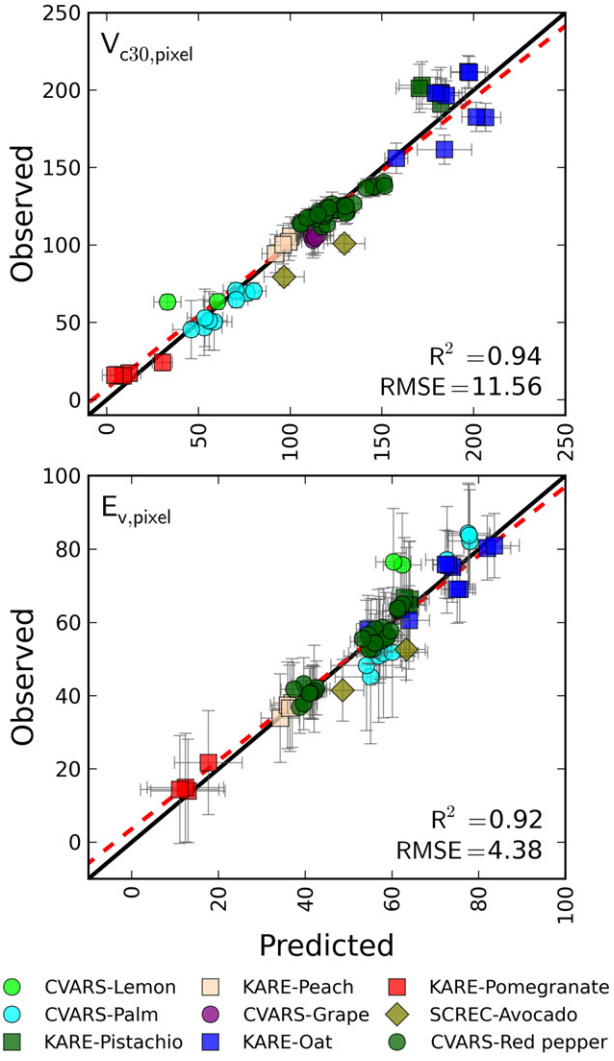

Fig. 2. Observed vs. predicted values for the 500 PLSR permutations to predict $V_{c30,pixel}$ (top, units μmol [m^{-2} ground area] s^{-1}) and $E_{v,pixel}$ (bottom, units kJ mol^{-1} K^{-1}). Cross-validation results are for the 25% of the data withheld from each of the 500 permutations, with error bars in the x-axis direction showing the range of prediction estimates for each data point across the 500 permutations, and error bars in the y-direction showing the range of the parameter estimate derived from the field data based on derivation of V_{c30} following Long and Bernacchi (2003) and E_v using the Arrhenius equation. In each panel, the red dashed line represents the relationship between observed and predicted values, while the solid black line represents to the 1:1 line. For both $V_{c30,pixel}$ and $E_{v,pixel}$, the slope and intercept of this trend did not differ significantly from 1 and 0, respectively.

4. Discussion

Results of this study provide evidence that the PLSR-based spectroscopic approach for estimating V_{cmax} proposed by Serbin et al. (2012), and supported by Dillen et al. (2012) and Ainsworth et al. (2014), can be scaled from the leaf to the landscape scale. Moreover, this work suggests that this approach can effectively produce spatially and temporally rich and coherent maps of photosynthetic variation across a fairly diverse array of C_3 agronomic plant taxa. Moreover, the current work points to the ability to remotely sense spatial variation in E_V, the temperature sensitivity of V_{cmax}. This is critically important because, when leaf temperature varies temporally or spatially by more than a few °C, the magnitude of error resulting from uncertainty in E_V can match or exceed that stemming from uncertainty in temperature-normalized V_{cmax}. The ability to map E_V provides a basis to characterize the acclimation of photosynthesis through space and time, e.g. with respect to changing environmental conditions or across gradients, such as those in elevation, nutrient availability, or disturbance legacies.

Despite differences in the scale of inquiry (leaf spectroscopy vs. canopy/image), our findings share broad similarities with those of Serbin et al. (2012) and Ainsworth et al. (2014). For instance, in both leaf-level studies and this work, the PLSR coefficients and VIP statistics across wavelengths are consistent with our current understanding of how vegetation optical properties relate to foliar biochemistry and physiology. Here, V_{c30} and E_V both appear to have strong relationships with reflectance at the red-edge (704 and 724 nm respectively), as does V_{c30} at 740–743 nm. The negative relationship of V_{c30} with the red-edge region points to the well-understood phenomenon that, compared to less vigorous vegetation, healthy green vegetation absorbs radiation at longer red wavelengths. This suggests that the red edge extends further into far-red wavelengths with increasing V_{cmax}, as indicated by Dillen et al. (2012). The positive relationship between V_{c30} and reflectance around 743 nm is particularly intriguing, as this could indicate an association with chlorophyll fluorescence, which under ambient conditions would be expected to increase with higher photosynthetic capacity (Zhang et al., 2014). This relationship is speculative and requires further study, but may be relevant to current research on the use of solar-induced chlorophyll fluorescence (SIF) in the far-red region to characterize photosynthetic metabolism (Campbell, Middleton, Corp, & Kim, 2008; Guanter et al., 2014; Joiner,

Table 2
Results of the PLSR modeling and cross-validation for $E_{v,pixel}$ and $V_{c30,pixel}$.

Property	Number of PLSR components	Calibration		Validation		Model-averaged	
		R^2	RMSE	R^2	RMSE	R^2	RMSE
$E_{v,pixel}$	3	0.93	4.14	0.90	5.02	0.92	4.38
$V_{c30,pixel}$	7	0.95	10.35	0.90	14.87	0.94	11.54

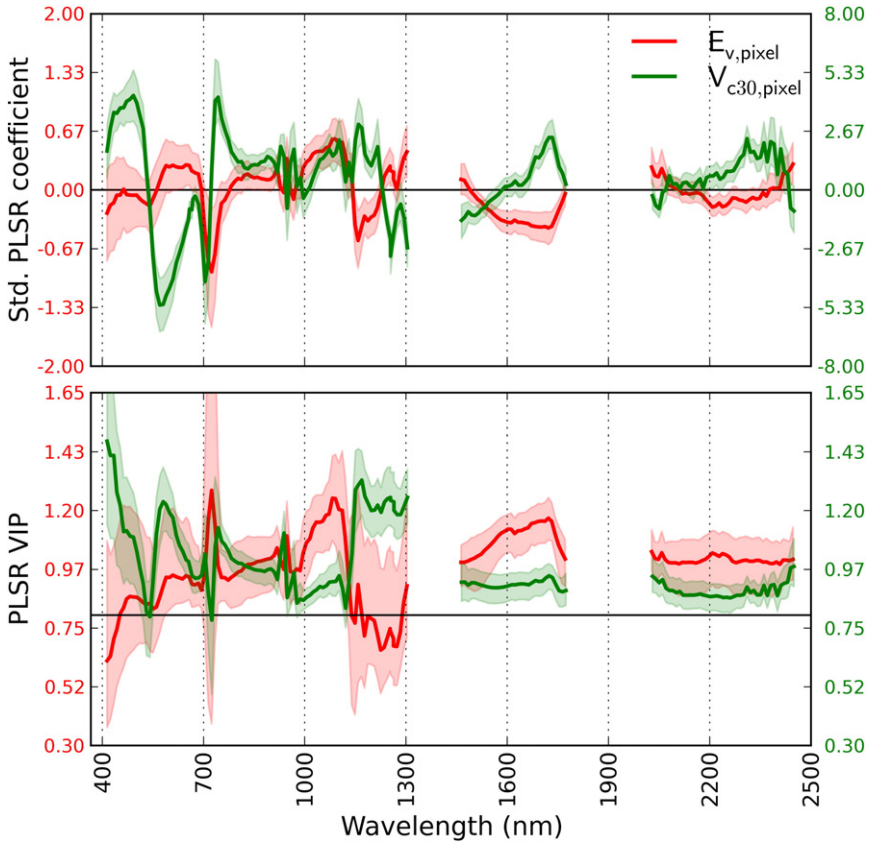

Fig. 3. Standardized PLSR coefficients (top) and Variable Importance of Projection (VIP, Wold, 1994) by wavelength to predict $V_{c30,pixel}$ and $E_{v,pixel}$. Gaps indicate atmospheric water absorption bands deleted from the statistical analyses. Solid lines indicate coefficients or VIP values of the mean model of the 500 permutations for each parameter, while the shaded areas indicate the 5% and 95% bounds of all 500 permutations. For standardized coefficients, shaded areas at wavelengths that bound zero indicate comparatively lower statistical contribution to the prediction for those wavelengths. Following Wold (1994), VIP values > 0.8 (solid horizontal black line) indicate high importance to the PLSR model.

Yoshida, Vasilkov, Corp, & Middleton, 2011; Rascher et al., 2009; Zhang et al., 2014).

Examining the patterns in Fig. 3 yields additional insights into the relationship between optical properties and photosynthetic functioning. For example, the strongly negative relationship of E_V to red-edge reflectance suggests that photosynthetic metabolism becomes less sensitive to temperature as vegetation vigor decreases and red-edge shifts to shorter wavelengths. Since higher E_V for a plant means a more rapid increase in photosynthetic capacity as leaf temperature rises, a shift in red-edge to higher wavelengths corresponds with greater capacity to respond photosynthetically to increased temperatures.

Some of the specific wavelength regions that we found to be related to these physiological parameters correspond to regions also found to be important to biochemical and structural foliar traits (e.g., Singh et al., in press) known to influence photosynthetic mechanism. The shape and direction of our standardized coefficients for V_{c30} generally track those of %N in the SWIR reported by Singh et al. (in press), especially in the shorter SWIR wavelengths (1463–1772 nm), with particular emphasis on a feature at 1722–1732 nm that has been identified as important in other studies (e.g., Martin et al., 2008; Serbin et al., 2012, 2014). The general importance of SWIR wavelengths to the estimation of key physiological traits in previous studies (Ainsworth et al., 2014; Serbin et al., 2012) is consistent with our mapping of V_{c30} shown here (e.g., Fig. 3 here, Fig. 4 in Serbin et al., 2012).

Coordination in leaf properties (Wright et al., 2004) and metabolic biochemistry (Curran, 1989; Elvidge, 1990;Serbin et al., 2012, 2014) also supports a mechanistic interpretation of our derived relationships for V_{c30}. For example, specific leaf area (or its inverse, leaf mass per area, LMA) and nitrogen concentration (%N) together broadly correlate with V_{cmax} (Kattge et al., 2009; Niinemets et al., 2006; Serbin et al., 2012). Higher %N can be interpreted as conferring a greater photosynthetic capacity due to its importance as a component of the enzyme rubisco, while lower LMA (thinner leaves) corresponds to greater leaf investment in photosynthetic productivity relative to leaf longevity (Wright et al., 2004). The VIP and standardized coefficients we report (Fig. 3) identify wavelength regions that Singh et al. (in press) also showed as important to mapping %N and LMA using comparable AVIRIS data. For example, Singh et al. (in press) demonstrated a strong negative relationship with %N at the red-edge (Singh et al., in press, Figs. 5 and 6). Similarly, high VIP and standardized coefficients for %N and LMA around 1158–1168 nm correspond to important wavelengths identified here (Fig. 3).

Whereas our ability to map V_{c30} is partly a function of its relationship to LMA and %N, which are mappable using imaging spectroscopy (Singh et al., in press), the potential to map E_V has no demonstrated mechanistic basis or empirical link with other leaf traits (Dillaway & Kruger, 2010). As a consequence, relationships between reflectance and E_V are more difficult to interpret. While correlations between E_V and red-edge position lend themselves to broad inference, other relationships clearly suggest the need for new, targeted studies. For example, the importance of the SWIR wavelengths matches our general expectations based on previous work (e.g. Ainsworth et al., 2014; Doughty, Asner, & Martin, 2011; Serbin et al., 2012), but the generally negative standardized coefficients for SWIR wavebands differs from the relationships with V_{c30} (this study) and %N (Singh et al., in press).

We believe that the work summarized in this study represents a significant step in the development of a unique remote-sensing capability, but it also contains a few important caveats. Specifically, the spectral response of a vegetated pixel is a function not just of plant tissue optical properties (i.e., chemistry, intercellular structure and physiology), but

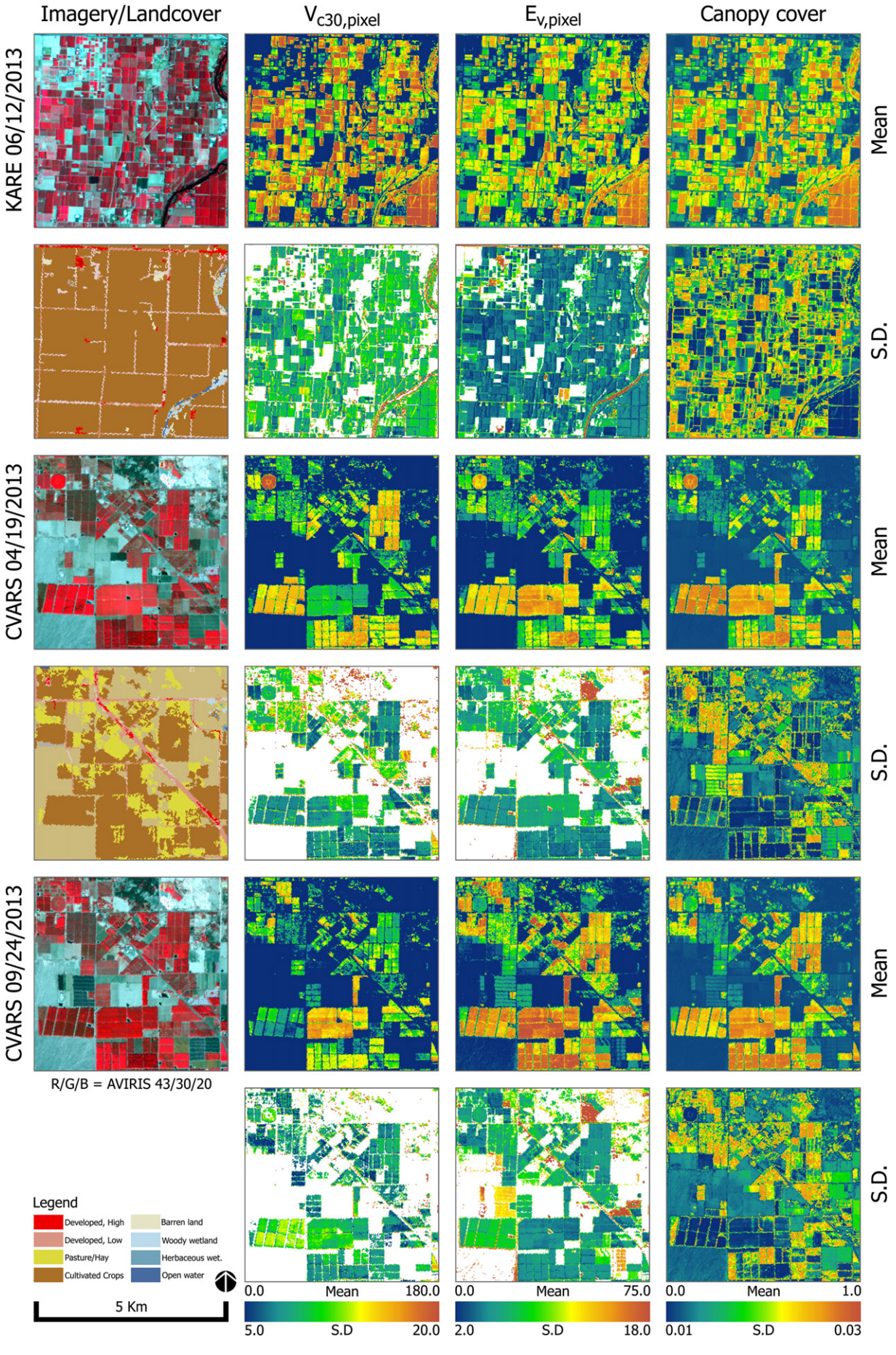
Imagery/Landcover
$V_{c30,pixel}$
$E_{v,pixel}$
Canopy cover
KARE 06/12/2013
CVARS 04/19/2013
CVARS 09/24/2013
Mean
S.D.
R/G/B = AVIRIS 43/30/20
Legend
Developed, High
Developed, Low
Pasture/Hay
Cultivated Crops
Barren land
Woody wetland
Herbaceous wet.
Open water
5 Km
0.0 Mean 180.0
5.0 S.D 20.0
0.0 Mean 75.0
2.0 S.D 18.0
0.0 Mean 1.0
0.01 S.D 0.03

also vegetation water content, leaf area index and morphology, canopy structure, species composition, phenology and pixel soil properties. The effects of these contributors to vegetation spectra also vary across the electromagnetic spectrum, as, for example, canopy structure has a very strong effect in the NIR compared to other wavelengths. Thus, we acknowledge that the inference space of our study is confined to comparatively simple, monospecific agroecosystems comprising C_3 broadleaf species. In addition to lacking some of the challenges brought about by canopy structural complexity (e.g., Knyazkhin et al., 2013), these ecosystems are managed to minimize biotic and abiotic stresses (e.g., insect and pathogen damage, drought, nutrient deficiencies) that might otherwise confound the interpretation of reflectance spectra (e.g., Close & Beadle, 2003; Stone, Chisholm, & Coops, 2001). Accordingly, our next goal is to broaden the analysis by including data collected in 2013–14 from natural ecosystems arrayed along pronounced elevation and climatic gradients, namely desert, pinyon–juniper, coastal sage, oak–pine savanna, and low-, mid- and high-elevation, conifer-dominated forest. Notably, all of these compositionally and structurally complex ecosystems had been subjected to protracted drought stress at the time of our sampling campaigns. Moreover, we are continuing to explore and contrast the role of biochemistry and leaf morphology and spectra in the ability to capture variation in V_{cmax}.

In our work, V_{c30} and E_V were scaled to the pixel level by proportionally modifying our estimates of these parameters using fractional vegetation cover (i.e., they are cover invariant). As such, our maps (Fig. 4) may show differences in pixel-level V_{c30} or E_V that, in fact, correspond to similar values of canopy-level V_{c30} and E_V once fractional vegetation cover is divided out of the estimate. Our results, and in particular the relationships between standardized coefficients/VIP and the physiological parameters that we interpret from Fig. 3, should thus be viewed with the caveat that the soil signal is an inherent component or source of uncertainty of the predictive equation (i.e. higher uncertainties in low-cover areas). On this point, we note that the PLSR method is well suited for our application because it is designed to handle noise in the predictor matrix (spectral observations) that is unrelated to the dependent trait of interest (Wold et al., 2001). Because leaf-level estimates of V_{c30} and E_V are of greater utility for modeling applications, these values can be retrieved using maps of proportional vegetation cover that we also demonstrate can be efficiently derived from hyperspectral imagery.

Our ability to map pixel-level V_{c30} and E_V—as well all as their uncertainties—represents a potentially important capacity to analyze spatial (and temporal) patterns of photosynthetic metabolism across landscapes using remote sensing. Importantly, this approach may allow us to step away from relying on mapping the determinants of photosynthetic capacity (e.g., %N and LMA) to mapping actual physiological parameters of interest, thus greatly reducing the dependence on ecological or physiological scaling functions. This capability would enable many opportunities for using imagery to test hypotheses about the fundamental controls and constraints on the spatial variation in photosynthetic processes. In addition, it would open up the potential for more explicit parameterization of EESMs. The potential to map E_V could also enable the prediction of dynamic or acclimatory responses of photosynthesis that are less tractable using the relationships between biochemistry and physiology (Kattge et al., 2009). Finally, the novelty of our findings and the as yet unknown mechanisms underlying our PLSR mapping results for E_V opens new opportunities to explore relationships among leaf optics, physiology and photosynthetic acclimation.

The patterns shown in Fig. 4 illustrate a number of important points, namely that V_{c30} and E_V do not fully track each other, and that these parameters can differ within agroecosystems and through time. We feel reasonably confident in our estimates, because areas with low vegetation cover (e.g., bare fields and the adjacent desert in CVARS) were predicted by the PLSR equations to have V_{c30} and E_V estimates close to zero (Fig. 4). This suggests that the PLSR models and AVIRIS spectra do capture inherent properties of vegetation physiology and biochemistry, since areas with no vegetation would not be expected to exhibit physiological capacity. Our use of uncertainty maps (Fig. 4) also illustrates the domain of our interpretations. Areas of vegetation mapped with higher uncertainties indicate those locations where the AVIRIS-retrieved spectra deviate from the domain of measurement in the field, either in terms of the physiological parameters V_{c30} and E_V, vegetation cover, or, potentially, the crop species. We believe the utility of our PLSR models will be enhanced when a more diverse range of species (both crops and natural vegetation) is included in expanded analyses.

Finally, we should note that the present study does not utilize available data on pixel surface temperature acquired simultaneously with AVIRIS imagery using the MODIS/ASTER airborne simulator (MASTER). These data provide an opportunity to estimate canopy surface temperature, which could then be readily combined with simultaneous estimates of canopy V_{c30} and E_V to characterize spatial and temporal dynamics in V_{cmax} under ambient environmental conditions. It is important to emphasize that knowledge of V_{c30} (i.e., V_{cmax} at 30 °C leaf temperature) and E_V (the temperature sensitivity of V_{cmax}) facilitates estimation of V_{cmax} at any leaf temperature; leaf or canopy surface temperatures can potentially be derived from thermal IR imagery, suggesting that concurrent hyperspectral and thermal IR imagery may offer a tremendous opportunity to capture both vegetation metabolic capacity and instantaneous vegetation metabolism. Ultimately, with an expanded data set across a larger diversity of plant species and sites, we will be able to explore the capacity to remotely characterize V_{cmax} and its temperature sensitivity for the entire canopy, rather than just its surface, using radiative transfer models (e.g., Zhang et al., 2014).

5. Conclusion

Our proposed method for predicting canopy surface V_{cmax} and its temperature sensitivity (E_V) complements, rather than supplants, the existing suite of approaches that employ remote sensing to characterize various aspects of canopy photosynthetic performance (e.g., Anderson et al., 2008; Carter, 1998; Gamon, Serrano, & Surfus, 1997; Grace et al., 2007; Hilker et al., 2008; Sims, Rahman, Cordova, et al., 2008; Zarco-Tejada, Pushnik, Dobrowski, & Ustin, 2003). Indeed, ours is one of several emerging strategies that use remotely sensed data to address current difficulties in accurately characterizing V_{cmax} variation at broad spatiotemporal scales (e.g., Zhang et al., 2014; Zhou et al., 2014). The work presented here was conducted in agricultural landscapes, and we can readily envision the potential of our method to improve yield forecasting and facilitate real-time monitoring of crop physiological status. On the whole, though restricted to broadleaf agricultural crops in terms of inference space, our findings point to the considerable promise of airborne and, by implication, space-borne imaging spectroscopy from the proposed HyspIRI mission as a tool to accurately estimate a key driver of canopy photosynthetic metabolism, and its sensitivity to climate variation, in terrestrial vegetation. Our results suggest that a global imaging spectrometer such as HyspIRI would offer the opportunity to characterize variations in photosynthetic capacity in space and time and learn how that capacity changes with environment. The specific prospect for agricultural monitoring and

Fig. 4. Maps derived from the analyses for three images in 2013, showing Kearney (KARE, image date 12 June) and two dates at Coachella Valley (CVARS, image dates 19 April and 24 September). Left column shows false color AVIRIS image for each date and NLCD land cover, followed by $V_{c30,pixel}$, $E_{v,pixel}$ and fractional canopy cover. Rows are labeled either "Mean" for the mean parameter prediction of the 500 permutations or "S.D." for the uncertainty of the prediction, expressed as the standard deviation of the 500 permutations. Dark blue areas in the $V_{c30,pixel}$, $E_{v,pixel}$ and canopy cover maps (far right, fourth column) have zero vegetation cover, but are not masked; however for clarity, these areas are masked out to white in the $V_{c30,pixel}$ and $E_{v,pixel}$ uncertainty maps because these areas would not be expected to exhibit any photosynthetic metabolism due to the absence of vegetation.

management in response to environmental drivers is considerable, and—if transferrable to other ecosystems—will facilitate greater understanding and characterization of vegetation function at a global scale.

Supplementary data to this article can be found online at http://dx.doi.org/10.1016/j.rse.2015.05.024.

Acknowledgments

This research was funded by NASA HyspIRI grant NNX12AQ28G. Thanks to Ben Spaier, Ryan Geygan, Ryan Sword, Rob Phetteplace, and Bethany Helzer for assistance with fieldwork, and Andy Ciurro with assistance in GIS data management. For facilitating this work, we also thank Mark Nickerson (Prime Time International) and staff members at the following University of California research stations: Kearney Agricultural Research and Extension Center (Chuck Boldwyn), Coachella Valley Agricultural Research Station (Vince Samons), and South Coast Research and Extension Center (Darren Haver). We gratefully acknowledge the contributions of two anonymous reviewers, which greatly improved an earlier version of this manuscript.

References

Ainsworth, E.A., Rogers, A., & Leakey, A.D.B. (2008). Targets for crop biotechnology in a future high-CO(2) and high-O(3) world. *Plant Physiology*, *147*, 13–19.

Ainsworth, E.A., Serbin, S.P., Skoneczka, J.A., & Townsend, P.A. (2014). Using leaf optical properties to detect ozone effects on foliar biochemistry. *Photosynthesis Research*, *119*, 65–76, http://dx.doi.org/10.1007/s11120-013-9837-y.

Anderson, M.C., Norman, J.M., Kustas, W.P., Houborg, R., Starks, P.J., & Agam, N. (2008). A thermal-based remote sensing technique for routine mapping of land-surface carbon, water and energy fluxes from field to regional scales. *Remote Sensing of Environment*, *112*, 4227–4241.

Asner, G.P., Martin, R.E., Anderson, C.B., & Knapp, D.E. (2015). Quantifying forest canopy foliar traits: Imaging spectroscopy versus field survey. *Remote Sensing of Environment*, *158*, 15–27.

Bernacchi, C.J., Bagley, J.E., Serbin, S.P., Ruiz-Vera, U.M., Rosenthal, D.M., & Vanloocke, A. (2013). Modelling C_3 photosynthesis from the chloroplast to the ecosystem. *Plant, Cell & Environment*, *36*, 1641–1657.

Campbell, E., Middleton, E.M., Corp, L.A., & Kim, M.S. (2008). Contribution of chlorophyll fluorescence to the apparent vegetation reflectance. *Science of the Total Environment*, *404*, 433–439.

Carter, G.A. (1998). Reflectance wavebands and indices for remote estimation of photosynthesis and stomatal conductance in pine canopies. *Remote Sensing of Environment*, *63*, 61–72.

Close, D. C., & Beadle, C. L. (2003). The ecophysiology of foliar anthocyanin. *Botanical Review*, *69*, 149–161.

Curran, P.J. (1989). Remote-sensing of foliar chemistry. *Remote Sensing of Environment*, *30*, 271–278.

Dahlin, K.M., Asner, G.P., & Field, C.B. (2013). Environmental and community controls on plant canopy chemistry in a Mediterranean-type ecosystem. *Proceedings of the National Academy of Sciences*, *110*, 6895–6900.

Dietze, M.C., Serbin, S.P., Davidson, C., Desai, A.R., Feng, X., Kelly, R., et al. (2014). A quantitative assessment of a terrestrial biosphere model's data needs across North American biomes. *Journal of Geophysical Research — Biogeosciences*, *119*, 286–300.

Dillaway, D.N., & Kruger, E.L. (2010). Thermal acclimation of photosynthesis: A comparison of boreal and temperate tree species along a latitudinal transect. *Plant, Cell & Environment*, *33*, 888–899.

Dillen, S., Op de Beeck, M., Hufkens, K., Buonanduci, M., & Phillips, N. (2012). Seasonal patterns of foliar reflectance in relation to photosynthetic capacity and color index in two co-occurring tree species, *Quercus rubra* and *Betula papyrifera*. *Agricultural and Forest Meteorology*, *160*, 60–68.

Domingues, T.F., Meir, P., Feldpausch, T.R., Saiz, G., Veenendaal, E.M., Schrodt, F., et al. (2010). Co-limitation of photosynthetic capacity by nitrogen and phosphorus in West Africa woodlands. *Plant, Cell & Environment*, *33*, 959–980.

Doughty, C., Asner, G., & Martin, R. (2011). Predicting tropical plant physiology from leaf and canopy spectroscopy. *Oecologia*, *165*, 289–299.

Dungan, R.J., Turnbull, M.H., & Kelly, D. (2007). The carbon costs for host trees of a phloem-feeding herbivore. *Journal of Ecology*, *95*, 603–613.

Elvidge, C. D. (1990). Visible and near-infrared reflectance characteristics of dry plant materials. *International Journal of Remote Sensing*, *11*, 1775–1795.

Farquhar, G.D., von Caemmerer, S., & Berry, J.A. (1980). A biochemical model of photosynthetic CO_2 assimilation in leaves of C_3 species. *Planta*, *149*, 78–90.

Feilhauer, H., Asner, G.P., Martin, R.E., & Schmidtlein, S. (2010). Brightness-normalized partial least squares regression for hyperspectral data. *Journal of Quantitative Spectroscopy and Radiative Transfer*, *111*, 1947–1957.

Frankenberg, C., O'Dell, C., Berry, J., Guanter, L., Joiner, J., et al. (2014). Prospects for chlorophyll fluorescence remote sensing from the Orbiting Carbon Observatory-2. *Remote Sensing of Environment*, *147*, 1–12.

Friedlingstein, P., Meinshausen, M., Arora, V.K., Jones, C.D., Anav, A., Liddicoat, S.K., et al. (2014). Uncertainties in CMIP5 climate projections due to carbon cycle feedbacks. *Journal of Climate*, *27*, 511–526.

Gamon, J.A., Serrano, L., & Surfus, J.S. (1997). The photochemical reflectance index: An optical indicator of photosynthetic radiation use efficiency across species, functional types, and nutrient levels. *Oecologia*, *112*, 492–501.

Geladi, P., & Kowalski, B.R. (1986). Partial least-squares regression — A tutorial. *Analytica Chimica Acta*, *185*, 1–17.

Grace, J., Nichol, C., Disney, M., Lewis, P., Quaife, T., et al. (2007). Can we measure terrestrial photosynthesis from space directly, using spectral reflectance and fluorescence? *Global Change Biology*, *13*, 1484–1497.

Green, R.O., Eastwood, M.L., Sarture, C.M., et al. (1998). Imaging spectroscopy and the Airborne Visible Infrared Imaging Spectrometer (AVIRIS). *Remote Sensing of Environment*, *65*, 227–248.

Grossman, Y.L., Ustin, S.L., Jacquemoud, S., Sanderson, E.W., Schmuck, G., et al. (1996). Critique of stepwise multiple linear regression for the extraction of leaf biochemistry information from leaf reflectance data. *Remote Sensing of Environment*, *56*, 182–193.

Guanter, L., Zhang, Y., Jung, M., Joiner, J., Voigt, M., et al. (2014). Global and time-resolved monitoring of crop photosynthesis with chlorophyll fluorescence. *Proceedings of the National Academy of Sciences*, *111*, E1327–E1333, http://dx.doi.org/10.1073/pnas.1320008111.

Hikosaka, K., Ishikawa, K., Borjigidai, A., Muller, O., & Onoda, Y. (2006). Temperature acclimation of photosynthesis: Mechanisms involved in the changes in temperature dependence of photosynthetic rate. *Journal of Experimental Botany*, *57*, 291–302.

Hilker, T., Coops, N.C., Hall, F.G., Black, T.A., Chen, B., et al. (2008). A modeling approach for upscaling gross ecosystem production to the landscape scale using remote sensing data. *Journal of Geophysical Research — Biogeosciences*, *113*, G03006, http://dx.doi.org/10.1029/2007JG000666.

Joiner, J., Yoshida, Y., Vasilkov, A.P., Corp, L.A., & Middleton, E.M. (2011). First observations of global and seasonal terrestrial chlorophyll fluorescence from space. *Biogeosciences*, *8*, 637–651.

Kattge, J., & Knorr, W. (2007). Temperature acclimation in a biochemical model of photosynthesis: A reanalysis of data from 36 species. *Plant, Cell & Environment*, *30*, 1176–1190.

Kattge, J., Knorr, W., Raddatz, T., & Wirth, C. (2009). Quantifying photosynthetic capacity and its relationship to leaf nitrogen content for global-scale terrestrial biosphere models. *Global Change Biology*, *15*, 976–991.

Knyazkhin, Y., Schull, M.A., Stenberg, P., Mottus, M., Rautiainen, M., et al. (2013). Hyperspectral remote sensing of foliar nitrogen content. *Proceedings of the National Academy of Sciences*, *110*, E185–E192, http://dx.doi.org/10.1073/pnas.1210196109.

Kruse, F.A., Lefkoff, A.B., Boardman, J.B., Heidebrecht, K.B., Shapiro, A.T., et al. (1993). The spectral image processing system (SIPS) — Interactive visualization and analysis of imaging spectrometer data. *Remote Sensing of Environment*, *44*, 145–163.

Kucharik, C.J., Foley, J.A., Delire, C., Fisher, V.A., Coe, M.T., et al. (2000). Testing the performance of a dynamic global ecosystem model: Water balance, carbon balance, and vegetation structure. *Global Biogeochemical Cycles*, *14*, 795–825.

Leuning, R. (2002). Temperature dependence of two parameters in a photosynthesis model. *Plant Cell and Environment*, *25*, 1205–1210.

Long, S.P., & Bernacchi, C.J. (2003). Gas exchange measurements, what can they tell us about the underlying limitations to photosynthesis? Procedures and sources of error. *Journal of Experimental Botany*, *54*, 2393–2401.

Martin, M.E., Plourde, L.C., Ollinger, S.V., Smith, M.L., & McNeil, B.E. (2008). A generalizable method for remote sensing of canopy nitrogen across a wide range of forest ecosystems. *Remote Sensing of Environment*, *112*, 3511–3519.

Medlyn, B.E., Dreyer, E., Ellsworth, D., et al. (2002a). Temperature response of parameters of a biochemically based model of photosynthesis. II. A review of experimental data. *Plant, Cell & Environment*, *25*, 1167–1179.

Medlyn, B.E., Loustau, D., & Delzon, S. (2002b). Temperature response of parameters of a biochemically based model of photosynthesis. I. Seasonal changes in mature maritime pine (*Pinus pinaster* Ait.). *Plant, Cell & Environment*, *25*, 1155–1165.

Medvigy, D., Wofsy, S.C., Munger, J.W., Hollinger, D.Y., & Moorcroft, P.R. (2009). Mechanistic scaling of ecosystem function and dynamics in space and time: Ecosystem demography model version 2. *Journal of Geophysical Research*, *114*, G01002.

Niinemets, U., Cescatti, A., Rodeghiero, M., & Tosens, T. (2006). Complex adjustments of photosynthetic potentials and internal diffusion conductance to current and previous light availabilities and leaf age in Mediterranean evergreen species *Quercus ilex*. *Plant, Cell & Environment*, *29*, 1159–1178.

Rascher, U., Agati, G., Alonso, L., Cecchi, G., Champagne, S., et al. (2009). CEFLES2: The remote sensing component to quantify photosynthetic efficiency from the leaf to the region by measuring sun-induced fluorescence in the oxygen absorption bands. *Biogeosciences*, *6*, 1181–1198.

Roberts, D.A., Quattrochi, D.A., Hulley, G.C., Hook, S.J., & Green, R.O. (2012). Synergies between VSWIR and TIR data for the urban environment: An evaluation of the potential for the Hyperspectral Infrared Imager (HyspIRI) Decadal Survey mission. *Remote Sensing of Environment*, *117*, 83–101.

Rogers, A. (2014). The use and misuse of Vc, max in Earth System Models. *Photosynthesis Research*, *119*, 15–29.

Sage, R.F., Way, D.A., & Kubien, D.S. (2008). Rubisco, rubisco activase, and global climate change. *Journal of Experimental Botany*, *59*, 1581–1595.

Schaefer, K., Schwalm, C.R., Williams, C., Arain, M.A., Barr, A., Chen, J.M., et al. (2012). A model-data comparison of gross primary productivity: Results from the North American Carbon Program site synthesis. *Journal of Geophysical Research, Biogeosciences*, *117*, G03010.

Serbin, S.P., Dillaway, D.N., Kruger, E.L., & Townsend, P.A. (2012). Leaf optical properties reflect variation in photosynthetic metabolism and its sensitivity to temperature. *Journal of Experimental Botany*, *63*, 489–502, http://dx.doi.org/10.1093/jxb/err294.

Serbin, S.P., Singh, A., McNeil, B.E., Kingdon, C.C., & Townsend, P.A. (2014). Spectroscopic determination of leaf morphological and biochemical traits for northern temperate and boreal tree species. *Ecological Applications*, *24*, 1651–1669, http://dx.doi.org/10.1890/13-2110.1.

Sims, D.A., Rahman, A.F., Cordova, V.D., et al. (2008). A new model of gross primary productivity for North American ecosystems based solely on the enhanced vegetation index and land surface temperature from MODIS. *Remote Sensing of Environment*, *112*, 1633–1646.

Singh, A., Serbin, S. P., McNeil, B. E., Kingdon, C. C., & Townsend, P. A. (2015). Imaging spectroscopy algorithms for mapping canopy foliar chemical and morphological traits and their uncertainties. *Ecological Applications*, http://dx.doi.org/10.1890/14-2098.1 (in press).

Stone, C., Chisholm, L., & Coops, N. (2001). Spectral reflectance of eucalypt foliage damaged by insects. *Australian Journal of Botany*, *49*, 687–698.

Thompson, D.R., Gao, B. -C., Green, R.O., Roberts, D.A., Dennison, P.E., & Lundeen, S.R. (2015). Atmospheric correction for global mapping spectroscopy: ATREM advances for the HyspIRI preparatory campaign. *Remote Sensing of Environment*, http://dx.doi.org/10.1016/j.rse.2015.02.010.

Weston, D.J., & Bauerle, W.L. (2007). Inhibition and acclimation of C_3 photosynthesis to moderate heat: a perspective from thermally contrasting genotypes of *Acer rubrum* (red maple). *Tree Physiology*, *27*, 1083–1092.

Wilson, K. B., Baldocchi, D. D., & Hanson, P. J. (2000). Spatial and seasonal variability of photosynthetic parameters and their relationship to leaf nitrogen in a deciduous forest. *Tree Physiology*, *20*, 565–578.

Wilson, J.B. (2011). Cover plus: Ways of measuring plant canopies and the terms used for them. *Journal of Vegetation Science*, *22*, 197–206.

Wold, S. (1994). PLS for multivariate linear modeling. In H. Waterbeemd, H. Timmerman, R. Mannhold, & P. Kroqsgaard-Larsen (Eds.), *QSAR: Chemometric methods in molecular design. Methods and Principles in Medicinal Chemistry*. (pp. 359). Wiley.

Wold, S., Ruhe, A., Wold, H., & Dunn, W.J. (1984). The collinearity problem in linear-regression — The partial least-squares (Pls) approach to generalized inverses. *SIAM Journal on Scientific and Statistical Computing*, *5*, 735–743.

Wold, S., Sjostrom, M., & Eriksson, L. (2001). PLS-regression: A basic tool of chemometrics. *Chemometrics and Intelligent Laboratory Systems*, *58*, 109–130.

Wright, I.J., Reich, P.B., Westoby, M., Ackerly, D., Baruch, Z., et al. (2004). The worldwide leaf economics spectrum. *Nature*, *428*, 821–827.

Wullschleger, S. D. (1993). Biochemical limitations to carbon assimilation in C3 plants - A retrospective analysis of the A/Ci curves from 109 species. *Journal of Experimental Botany*, *44*, 907–920.

Wullschleger, S.D., Epstein, H.E., Box, E.O., Euskirchen, E.S., Goswami, S., Iversen, C.M., et al. (2014). Plant functional types in earth system models: Past experiences and future directions for application of dynamic vegetation models in high-latitude ecosystems. *Annals of Botany*, *114*, 1–16.

Xu, L., & Baldocchi, D.D. (2003). Seasonal trends in photosynthetic parameters and stomatal conductance of blue oak (*Quercus douglasii*) under prolonged summer drought and high temperature. *Tree Physiology*, *23*, 865–877.

Zarco-Tejada, P.J., Pushnik, J.C., Dobrowski, S., & Ustin, S.L. (2003). Steady-state chlorophyll a fluorescence detection from canopy derivative reflectance and double-peak red-edge effects. *Remote Sensing of Environment*, *84*, 283–294.

Zhang, Y., Guanter, L., Berry, J.A., Joiner, J., van Der Tol, C., et al. (2014). Estimation of vegetation photosynthetic capacity from space-based measurements of chlorophyll fluorescence for terrestrial biosphere models. *Global Change Biology*, *20*, 3727–3742, http://dx.doi.org/10.1111/gcb.12664.

Zhou, Y., Ju, W., Sun, X., Hu, Z., Han, S., et al. (2014). Close relationship between spectral vegetation indices and V_{cmax} in deciduous and mixed forests. *Tellus B*, *66*, http://dx.doi.org/10.3402/tellusb.v66.23279.